

赵汇珍, 陈勇, 涂聪, 等. 柳江盆地髻髻山组凝灰岩地球化学与熔体包裹体水含量特征[J]. 岩矿测试, 2025, 44(1): 88-101. DOI: 10.15898/j.ykcs.202404030074.

ZHAO Huizhen, CHEN Yong, TU Cong, et al. Geochemical Characteristics and Water Content of Melt Inclusions in the Tuff of the Tiaojishan Formation, Liujiang Basin[J]. Rock and Mineral Analysis, 2025, 44(1): 88-101. DOI: 10.15898/j.ykcs.202404030074.

柳江盆地髻髻山组凝灰岩地球化学与熔体包裹体水含量特征

赵汇珍^{1,2}, 陈勇^{1,2*}, 涂聪³, 冯艳伟^{1,2}

(1. 中国石油大学(华东) 深层油气全国重点实验室, 山东 青岛 266580;

2. 中国石油大学(华东) 地球科学与技术学院, 山东 青岛 266580;

3. 中国科学技术大学地球和空间科学学院, 安徽 合肥 230026)

摘要: 水作为岩浆体系中最主要的挥发组分, 对岩浆的形成和演化有重要的影响, 柳江盆地髻髻山组岩浆岩是燕山期火山活动的重要产物, 尽管前人对其地球化学特征进行了大量研究, 但关于柳江盆地燕山期岩浆中的水含量仍不清楚。熔体包裹体记录了原始岩浆信息, 是获取岩浆水含量特征的最直接样品。本文基于全岩地球化学分析, 利用标准样品建立了显微激光拉曼光谱定量熔体包裹体水含量的标定曲线, 并对柳江盆地髻髻山组下部流纹质岩屑-晶屑凝灰岩中石英斑晶内的原生熔体包裹体进行了水含量定量分析。结果表明: 髻髻山组下部凝灰岩样品具有富 Si、Al、大离子亲石元素富集、高场强元素亏损、轻稀土富集、重稀土亏损、负 Eu 异常、Sr 含量低等特点; 熔体包裹体中水含量的定量分析结果为 0.99%~4.98%, 平均水含量为 2.62%, 与前人统计的酸性岩浆水含量基本一致。地球化学特征和熔体包裹体水含量分析结果共同揭示了研究区髻髻山期早期为富水酸性岩浆。结合髻髻山期样品的熔体包裹体水含量测定结果及其早期的大规模火山喷发背景, 本文认为岩浆中高含水量增强了岩浆系统的喷发动力, 是诱发研究区髻髻山期早期大规模火山爆发的有利因素之一。

关键词: 柳江盆地; 髻髻山组; 凝灰岩; 熔体包裹体; 水含量; 显微激光拉曼光谱法

要点:

(1) 标定曲线的建立是显微激光拉曼光谱法定量测定熔体包裹体水含量的关键。

(2) 熔体包裹体的水含量与拉曼光谱参数之间具有很好的线性关系, 应用少量标样即可建立标定曲线。

(3) 柳江盆地髻髻山组凝灰岩中熔体包裹体平均水含量为 2.62%, 属于酸性富水岩浆体系。

中图分类号: P575

文献标识码: A

水(H₂O)是自然岩浆体系中最主要的挥发组分, 显著影响岩浆的黏度、熔点和结晶行为, 从而控制岩浆分异演化的趋势^[1-3]。而熔体包裹体是在岩浆活动过程中捕获在结晶矿物晶格缺陷中的岩浆熔体^[4-5], 一定程度上保留了所捕获岩浆的组分状态, 可以提供岩浆作用过程的直接信息^[6-8]。前人通过大量研究证实了应用熔体包裹体确定岩浆挥发份的

可靠性^[2,8-10]。借助熔体包裹体研究岩浆中的挥发份含量, 不仅可以揭示岩浆的分异演化过程, 还能为理解岩浆活动特征提供重要依据。

目前应用于测定硅酸盐熔体包裹体中的 H₂O 的原位分析技术主要有^[11-12]: 电子探针(EPMA)、离子探针(SIMS)、傅里叶变换红外光谱和显微激光拉曼光谱。相较于其他方法, 显微激光拉曼光谱分

收稿日期: 2024-04-03; 修回日期: 2024-07-31; 接受日期: 2024-08-07; 网络出版日期: 2024-09-05

基金项目: 国家自然科学基金项目(41873070, 42173042)

第一作者: 赵汇珍, 硕士研究生, 地质学专业。E-mail: s22010030@s.upc.edu.cn。

通信作者: 陈勇, 博士, 教授, 长期从事流体包裹体地球化学与盆地成岩成藏流体相关研究。

E-mail: yongchenzy@upc.edu.cn。

析具有高空间分辨率、快速、无损分析、样品制备简单等优点^[13-15],可应用于分析暴露在表面或包裹于内部的样品,并且能够在 0%~20%(含水量)浓度范围内精确测定^[16-19]。Thomas^[16]利用显微激光拉曼光谱技术研究了 26 个已知成分的人工合成玻璃和天然硅酸盐熔体包裹体样品,在水含量 0%~16% 范围内获得与实测值基本一致的结果;Chabiron 等^[17]通过显微激光拉曼光谱法测试熔体包裹体水含量,该方法得到的结果与红外光谱测试结果基本一致;王玉琪等^[12]使用显微激光拉曼光谱快速标定了花岗质玻璃样品,其测试结果与红外光谱水含量结果的相对误差小于 10%;Tu 等^[19]建立了一种基于激光共聚焦拉曼光谱测定硅酸盐熔体中总溶解水及不同形态水含量的方法。上述研究进一步证实了显微激光拉曼光谱技术在测定熔体包裹体水含量方面的独特优势和可靠性。

髻髻山组火山岩是燕山造山带中生代最具代表性的钙碱性火山岩之一,代表了燕山期大规模火山喷发的开始^[20]。前人的研究主要集中在燕山造山带中生代火山岩的地球化学特征^[21-25],而水作为影响岩浆形成及演化的重要因素,目前对髻髻山组火山岩中的水含量尚不清楚。柳江盆地向斜核部出露了中侏罗统髻髻山组(J_{2t})下部的凝灰岩^[24,26],作为火山活动早期产物,研究其岩浆中的水含量对于了解火山活动有重要意义。因此,对该凝灰岩开展岩石地球化学分析和岩浆水含量定量研究,可以为深入认识和理解该地区的岩浆活动提供重要依据。本文以柳江盆地侏罗系髻髻山组下部凝灰岩为研究对象,以岩石学、岩石地球化学和包裹体岩相学分析为基础,应用显微激光拉曼光谱法定量测定了凝灰岩中熔体包裹体的水含量,并讨论了岩浆中的水对火山喷发行为的影响。

1 研究区地质概况

柳江盆地位于河北省秦皇岛市,其大地构造位置位于华北陆块北缘中朝地块燕山褶皱造山带东段(图 1a)。盆地是一个近南北向不对称的短轴向斜(图 1b),西翼地层紧凑且直立倒转,东翼地层舒展而平缓,主要构造线偏于盆地西部,其走向大致为南北向。

柳江盆地髻髻山组地层岩性特征^[26]表现为:下部主要发育灰绿色、浅黄色的安山质、流纹质火山集块岩夹凝灰岩和火山熔岩;中部发育灰绿色安山质、角闪安山质、粗安山质火山熔岩与集块岩、角砾岩互层;上部发育黑绿色、紫红色、青灰色玄武质、

玄武安山质、辉石安山质火山熔岩与熔结集块岩、集块岩互层,夹有少量的火山角砾岩及凝灰岩。由下向上,岩性由偏酸性逐渐过渡为中性、中基性。

2 实验部分

2.1 样品及处理

本文所采集的凝灰岩样品取自河北省秦皇岛市柳江盆地髻髻山组下部野外露头。将采集的新鲜凝灰岩样品分别制备成厚约 0.03mm 的普通岩石薄片和厚约 0.1mm 双面抛光的流体包裹体薄片多张,用于显微观察和显微激光拉曼光谱测试。挑选新鲜的凝灰岩样品 2 块,用于全岩主量和微量元素分析。

2.2 样品测试

2.2.1 显微观察

样品的显微观察在中国石油大学(华东)深层油气全国重点实验室完成。镜下观察使用仪器为徕卡 DM2700P 显微镜,在透光条件下观察和记录样品的岩石学特征和熔体包裹体岩相学特征,并在镜下挑选、标记保存完好的熔体包裹体,以备显微激光拉曼光谱测试。

2.2.2 主量和微量元素分析

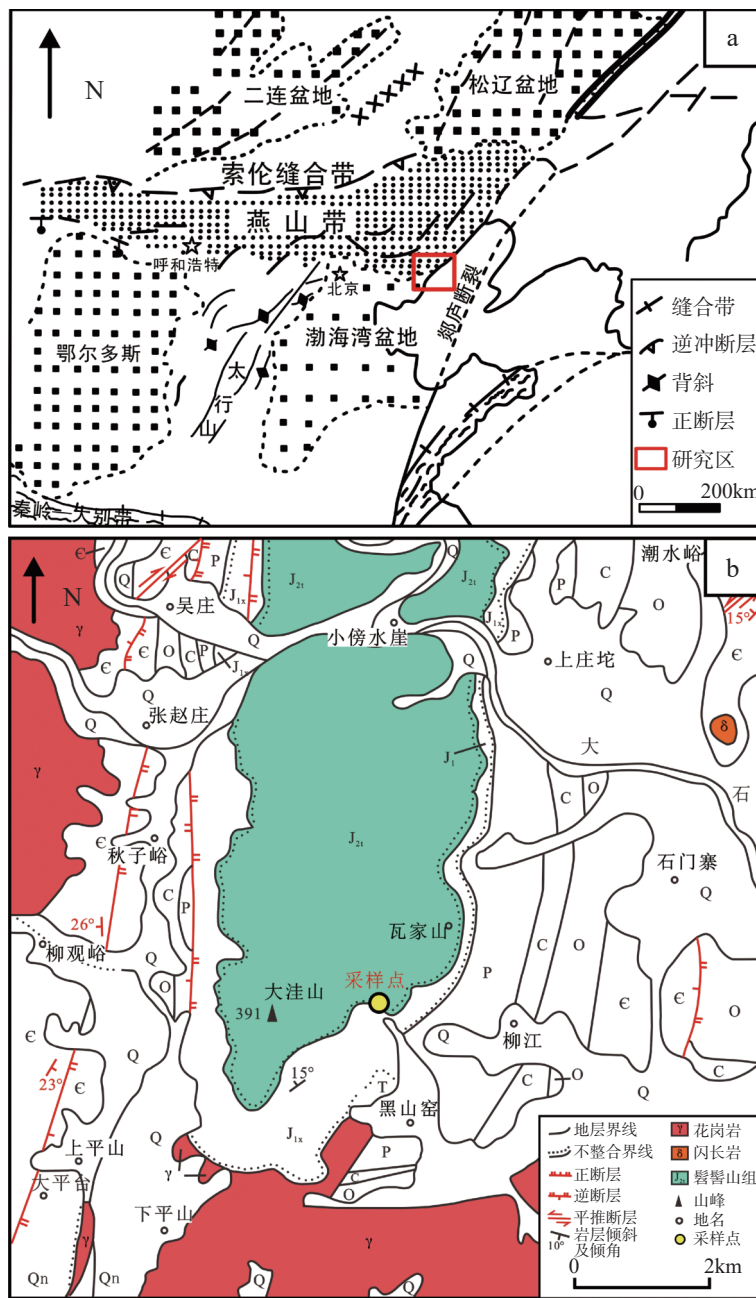
样品全岩主量和微量元素分析测试在中国石油大学(华东)深层油气全国重点实验室完成。全岩主量元素采用 IRIS Intrepid II XSP 电感耦合等离子体发射光谱仪(ICP-OES)进行测试;微量元素和稀土元素使用 ELAN9000 电感耦合等离子体质谱仪(ICP-MS)进行测试。用于本次测试的凝灰岩样品为 TJS-1 和 TJS-2,对每块样品分别进行两次测试,以保证数据可靠性,测试偏差小于 1%。

2.2.3 显微激光拉曼光谱分析

人工合成硅酸盐玻璃标准样品和髻髻山组熔体包裹体样品的显微激光拉曼光谱测试在中国石油大学(华东)深层油气全国重点实验室完成。用于测试的人工合成玻璃标样依次命名为标样 1~标样 4,熔体包裹体则按照 MI-1 至 MI-9 顺序依次编号。为降低实际样品薄片中的黏合剂对实验的干扰,测试前使用丙酮溶液浸泡清洗薄片,风干后进行实验测试分析。实验仪器为 LABRAM HR EVO 型激光拉曼光谱仪(法国 HORIBA FRANCE SAS 公司),使用的激光光源波长为 532nm,光栅 1800gr/mm,光谱分辨率 $\leq 0.65\text{cm}^{-1}$,测试精度小于 $\pm 0.1\text{cm}^{-1}$,实验环境温度为 20℃,湿度为 50%。

2.3 测试数据质量控制

显微激光拉曼光谱法定量熔体包裹体水含量的



(a) 研究区大地构造位置, 据郑亚东等 [27] 修编; (b) 研究区地质简图, 据吴孔友等 [26] 修编。

图1 研究区地质简图

Fig. 1 Geological diagrams of the research area (Figure a is modified after Zheng, et al [27] ; Figure b is modified after Wu, et al [26]).

准确性会受到拉曼光谱仪参数、拉曼图谱数据处理方法、标准样品、标定参数等方面的影响。因此, 本文在使用该方法进行熔体包裹体水含量定量分析时, 对上述四个方面的影响因素进行了优化, 从而提高实验测试结果的准确性和精度。

2.3.1 拉曼光谱参数设置

由于过高的激光功率和积分时间可能会导致玻璃中水的丢失 [11-12, 19], 通过比较不同条件下的水峰强度, 最终采用的实验条件为激光功率 30mW, 积分

时间 30s, 积分次数 3 次。在使用激光拉曼光谱仪对包裹体进行测试之前, 用单晶硅标准样对该仪器进行校正以确保实验结果的准确性。

2.3.2 拉曼图谱数据处理

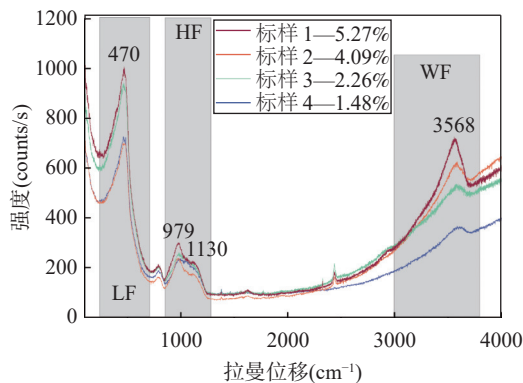
由于拉曼光谱在测试过程中会受到硅酸盐成分、仪器及测试环境等方面的影响, 需要对测试得到的拉曼光谱进行数据处理。本文结合强度校正和基线校正对实验获得的拉曼光谱进行校正, 以消除上述影响。具体校正程序见 2.4.2 节。

2.3.3 标准样品应用

为尽可能地提高测试结果准确性,在建立熔体包裹体中水的特征峰强度与浓度之间的线性关系时,首先需要借助标准物质建立实验室标定曲线。本文通过对中国科学技术大学壳幔物质与环境重点实验室人工合成的11个不同水含量的含水玻璃标准样品测试结果进行校正(包括11个参考样品^[19]和4个实测样品),建立了实验室水含量标定曲线。

2.3.4 参数标定

拉曼光谱仪定量限定硅酸盐玻璃水含量的校正方法包括外标法和内标法^[11,16]。相较于外标法,内标法在标定含水硅酸盐玻璃中水含量时更为准确且可靠,可以通过选取合适的标定参数和公式消除硅酸盐玻璃成分差异产生的影响^[11]。样品的岩石学和地球化学特征表明,髻髻山组凝灰岩为酸性火山岩,而酸性硅酸盐玻璃具有较强的 LF_{470} 拉曼峰高度/强度比(图2),优先选择 A_{WF}/A_{LF} 作为最佳标定参数^[11,19]。



红色实线为5.27% H_2O 人工合成标准样品的拉曼谱图;橙色实线为4.09% H_2O 人工合成标准样品的拉曼谱图;绿色实线为2.26% H_2O 人工合成标准样品的拉曼谱图;蓝色实线为1.48% H_2O 人工合成标准样品的拉曼谱图。 LF - $250\text{cm}^{-1} \sim 700\text{cm}^{-1}$ 为低波段谱带; HF - $850\text{cm}^{-1} \sim 1300\text{cm}^{-1}$ 为高波段谱带; WF - $3000\text{cm}^{-1} \sim 3800\text{cm}^{-1}$ 为总水谱带。

图2 不同水含量人工合成流纹质玻璃的拉曼光谱

Fig. 2 Raman spectra of artificially synthesized rhyolitic glasses with different water content.

2.4 熔体包裹体水含量定量分析

2.4.1 含水玻璃标样拉曼光谱特征谱带

人工合成含水玻璃标准样品由中国科学技术大学壳幔物质与环境重点实验室提供,标样1~标样4分别为5.27% H_2O 、4.09% H_2O 、2.26% H_2O 和1.48% H_2O 的实际测试样品,分别对应Tu等^[19]的样品RH-8、RH-7、RH-5和RH-4。对人工合成含水

玻璃标准样品进行显微激光拉曼光谱测试,拉曼光谱图显示,含水玻璃拉曼光谱具有三个特征谱带(图2),与前人实验结果一致^[16-17,19]。在硅酸盐玻璃的低波段谱带中,最明显的谱带在 470cm^{-1} 处,这是由于桥氧($T-O-T$; $T=Si, Al$)的弯曲振动引起的^[16-17]。而高波段谱带则与非桥氧($T-O$; $T=Si, Al$)的拉伸振动有关^[28-32]。在总水谱带中,在 $3540 \sim 3620\text{cm}^{-1}$ 的宽带则是因为 $O-H$ 和 H_2O_m 伸缩振动的共同作用^[33-34]。

2.4.2 拉曼图谱数据处理方法

使用Origin 2018软件对拉曼光谱图进行以下光谱处理。

第一步:强度校正。对原始拉曼光谱进行Long^[35]校正以获得真实的光谱强度,校正方程表示为:

$$I = I_{\text{obs}} \left\{ \frac{v_0^3 \left[1 - \exp\left(-\frac{hcv}{KT}\right) \right] v}{(v_0 - v)^4} \right\} \quad (1)$$

式中: I_{obs} 为测量强度; v_0 为入射激光的波数($v_0=18797\text{cm}^{-1}$); h 为普朗克常数($6.62607 \times 10^{-34}\text{J}\cdot\text{s}$); c 为光速($2.9979 \times 10^{10}\text{cm/s}$); K 为玻尔兹曼常数($1.38065 \times 10^{-23}\text{J/K}$); T 为绝对温度。

第二步,基线校正。根据样品的光谱特征分段式固定部分基线,而后使用三次样条插值法扣除基线。

第三步,谱带积分。含水玻璃拉曼光谱具有三个特征谱带,即 LF 、 HF 、 WF (图2),对基于前两步得到的拉曼光谱进行峰面积积分,分别得到 LF 、 HF 、 WF 的积分面积,简称为 A_{LF} 、 A_{HF} 、 A_{WF} 。

2.4.3 熔体包裹体水含量标定曲线

前人研究证明,硅酸盐玻璃的水含量与其拉曼参数之间存在良好的线性关系^[16-17,19],但由于不同激光拉曼光谱仪的效率因子不同,其线性关系的系数会存在差异。因此,不同仪器的 A_{WF}/A_{LF} 值之间也存在良好的线性关系。通过4个人工合成标准样品确定本文实际测量值 A_{WF}/A_{LF} 与Tu等^[19]测得的 A_{WF}/A_{LF}^* 之间的线性关系,可以得到11个标准样品的 A_{WF}/A_{LF} 值(表1),然后使用Origin 2018软件对标准样品进行 $A_{WF}/A_{LF}-C_{H_2O}$ 线性拟合,得到的熔体包裹体水含量(C_{H_2O})标定曲线如图3所示,其方程表示如下:

$$C_{H_2O} = 1.26 \times \left(\frac{A_{WF}}{A_{LF}} \right) \quad R^2 = 0.998 \quad (2)$$

表 1 不同水含量人工合成含水硅酸盐玻璃标准样品的积分面积等参数测量结果

Table 1 Measurement results of integrated area and other parameters of artificially synthesized water-containing silicate glasses standard samples with different water content.

人工合成含水玻璃 标准样品编号	A_{LF}	A_{WF}	A_{WF}/A_{LF}^* (Tu 等 ^[19] 测量值)	A_{WF}/A_{LF} (转换值或实测值)	C_{H_2O} (%)
RH-1(Tu 等, 2023)	/	/	1.0700	0.3726	0.33
RH-2(Tu 等, 2023)	/	/	1.3300	0.4631	0.41
RH-3(Tu 等, 2023)	/	/	1.8400	0.6407	0.58
RH-4(Tu 等, 2023)	/	/	3.2600	1.1351	1.48
RH-5(Tu 等, 2023)	/	/	4.9400	1.7201	2.26
RH-6(Tu 等, 2023)	/	/	6.3100	2.1971	3.01
RH-7(Tu 等, 2023)	/	/	8.5100	2.9632	4.09
RH-8(Tu 等, 2023)	/	/	11.7800	4.1018	5.27
RH-9(Tu 等, 2023)	/	/	14.3000	4.9793	6.35
RH-10(Tu 等, 2023)	/	/	15.4400	5.3762	6.84
RH-11(Tu 等, 2023)	/	/	21.3100	7.4201	9.05
标准样品 1	292.6424	1264.846	/	4.3222	5.27
标准样品 2	244.9186	776.2908	/	3.1696	4.09
标准样品 3	229.9241	374.9651	/	1.6308	2.26
标准样品 4	189.5898	250.3734	/	1.3206	1.48

注: RH-1 至 RH-11 为 Tu 等^[19]测试样品; 标样 1 至标样 4 为本文中的实际测试样品, 分别对应 Tu 等^[19]的样品 RH-8、RH-7、RH-5、RH-4。
“/”代表本文未使用的数据。

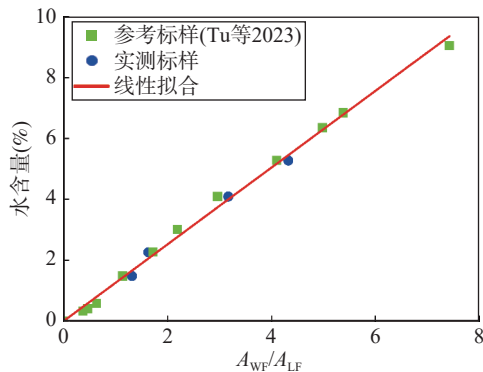


图3 含水流纹质玻璃水含量标定曲线

Fig. 3 Calibration curve for total water content in hydrous rhyolitic glasses.

3 结果与讨论

3.1 岩石学与地球化学特征

3.1.1 岩石学特征

样品新鲜面呈灰白色, 具凝灰结构、块状构造。岩石主要由晶屑 (35%)、岩屑 (25%) 和基质 (40%) 组成。晶屑成分以石英、长石为主, 粒径可达 1.8mm; 岩屑以流纹岩岩屑为主, 粒径约 0.5 ~ 2mm; 基质由尘屑和火山灰构成。镜下观察表明, 岩石发育凝灰结构、假流纹构造, 发生轻微蚀变。岩石定名为流纹质岩屑-晶屑凝灰岩。

3.1.2 岩石主量和微量元素地球化学特征

柳江盆地髻髻山组凝灰岩样品全岩主量元素分析结果见表 2。样品中 SiO_2 含量为 75.18% ~ 77.14%, Fe_2O_3 含量 1.06% ~ 2.28%, Al_2O_3 含量 12.61% ~ 13.02%, CaO 含量 0.14% ~ 1.10%, MgO 含量 0.65% ~ 1.29%, TiO_2 含量 0.14%, 全碱 (Na_2O+K_2O) 含量 4.04% ~ 4.24%, Na_2O/K_2O 值为 0.56 ~ 0.65。里特曼指数 (σ) 为 0.51 ~ 0.53, 属钙碱性系列。TAS 图解投图落在在流纹岩区域中 (图 4a), 符合样品中流纹质岩屑发育的岩石学特征, 表明研究区髻髻山组下部凝灰岩的形成与酸性岩浆活动之间存在密切联系。

柳江盆地髻髻山组凝灰岩样品全岩微量元素分析结果见表 3。原始地幔标准化蛛网图 (图 4b) 显示, 大离子亲石元素 (Rb、Th、U、K) 富集, 高场强元素 (Ta、Nb、Ti、Zr、P) 亏损, 具明显 Pb 正异常, Sr 负异常, 弱 Ba、La、Ce 负异常; 稀土元素球粒陨石标准化曲线 (图 4c) 呈海鸥式展布, 具明显 Eu 负异常, 说明岩浆演化过程中存在明显的斜长石分离结晶作用; 稀土元素配分模式为右倾型, 呈现轻稀土富集、重稀土亏损的特点。(La/Sm)_N 平均值为 6.77, (Gd/Yb)_N 平均值为 1.88, 表明轻稀土分馏程度高而重稀土分馏程度较低; (La/Yb)_N 平均值为 15.65, 轻重稀土分馏明显。李伍平等^[21]对燕山造山带中-晚侏罗世髻髻山期火山岩进行研究发现, 冀北髻髻山期流纹岩样

表 2 髻髻山组凝灰岩全岩主量元素测试结果

Table 2 Analytical results of major elements in tuff of the Tiaojishan Formation.

凝灰岩样品 编号	Na ₂ O (%)	MgO (%)	Al ₂ O ₃ (%)	SiO ₂ (%)	P ₂ O ₅ (%)	K ₂ O (%)	CaO (%)	TiO ₂ (%)	MnO (%)	Fe ₂ O ₃ (%)	烧失量 (%)	Na ₂ O+K ₂ O (%)	主量元素含量 合计 (%)
TJS-1	1.45	1.29	13.02	75.18	0.03	2.60	1.10	0.14	0.04	2.28	3.38	4.04	100.48
TJS-2	1.67	0.65	12.61	77.14	0.02	2.58	0.14	0.14	0.03	1.06	3.04	4.24	99.07

注: 为确保测试结果的可靠性, 实验数据取同一样品两次测试结果的平均值。

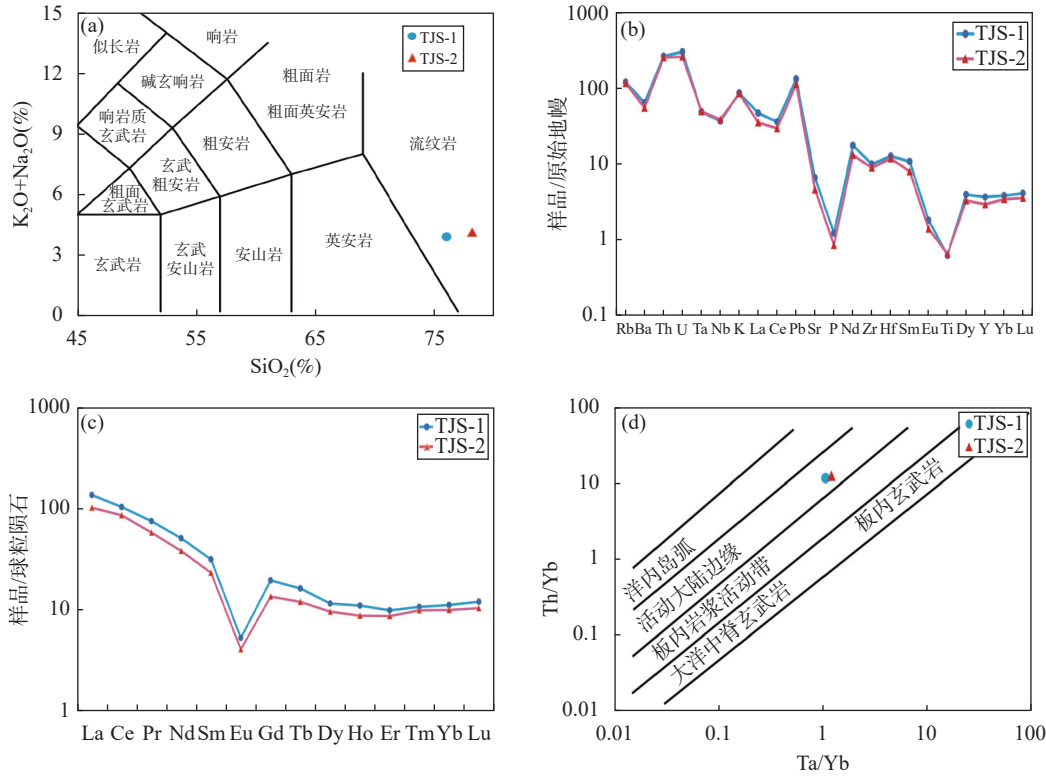


图 4 髻髻山组凝灰岩岩石地球化学特征

Fig. 4 Lithochemical characteristics of the tuff of the Tiaojishan Formation.

表 3 髻髻山组凝灰岩全岩微量元素测试结果

Table 3 Analytical results of trace elements in tuff of the Tiaojishan Formation.

凝灰岩样品 编号	Li (μg/g)	Be (μg/g)	B (μg/g)	Sc (μg/g)	V (μg/g)	Cr (μg/g)	Co (μg/g)	Ni (μg/g)	Cu (μg/g)	Zn (μg/g)	Ga (μg/g)	Ge (μg/g)	As (μg/g)	Rb (μg/g)	Sr (μg/g)
TJS-1	29.75	4.72	17.15	3.84	6.09	7.14	1.26	3.90	2.57	36.30	19.25	1.68	0.41	76.35	139.50
TJS-2	10.46	3.78	15.55	4.89	6.59	4.43	0.72	1.69	2.39	18.56	17.55	0.80	0.47	74.13	97.87
凝灰岩样品 编号	Y (μg/g)	Zr (μg/g)	Nb (μg/g)	Mo (μg/g)	Cd (μg/g)	Cs (μg/g)	Ba (μg/g)	La (μg/g)	Ce (μg/g)	Pr (μg/g)	Nd (μg/g)	Sm (μg/g)	Eu (μg/g)	Gd (μg/g)	Tb (μg/g)
TJS-1	16.75	112.50	26.30	2.24	0.09	1.39	451.50	32.45	63.90	7.16	23.90	4.84	0.31	4.04	0.61
TJS-2	13.50	100.77	27.64	1.80	0.04	0.99	386.05	24.29	52.86	5.53	17.92	3.56	0.24	2.80	0.45
凝灰岩样品 编号	Dy (μg/g)	Ho (μg/g)	Er (μg/g)	Tm (μg/g)	Yb (μg/g)	Lu (μg/g)	Hf (μg/g)	Ta (μg/g)	W (μg/g)	Tl (μg/g)	Pb (μg/g)	Bi (μg/g)	Th (μg/g)	U (μg/g)	
TJS-1	2.95	0.63	1.65	0.27	1.91	0.31	3.97	2.02	0.51	0.63	24.40	0.16	22.40	6.35	
TJS-2	2.45	0.50	1.44	0.25	1.70	0.27	3.68	2.04	0.70	0.60	20.70	0.10	21.60	5.50	

注: 为确保测试结果的可靠性, 实验数据取同一样品两次测试结果的平均值。

品具有轻稀土元素强烈富集、重稀土元素强烈亏损、负Eu异常、Sr含量低(94~135μg/g)等特征,与本研究中凝灰岩样品的岩石地球化学特征相似。Ta/Yb-Th/Yb图解(图4d)投点落在活动大陆边缘,指示该时期研究区受洋壳俯冲的影响,岩浆活动强烈。(La/Nb)_N平均值为1.06[原始地幔(La/Nb)_N值约为0.96,平均大陆壳(La/Nb)_N值为2.5^[39]],指示成岩过程中受到一定地壳混染作用。上述地球化学特征与前人的研究结果^[20,40-41]一致,即实验样品可以在一定程度上反映研究区髫髻山期早期的岩浆活动特征。

3.2 凝灰岩熔体包裹体与水含量特征

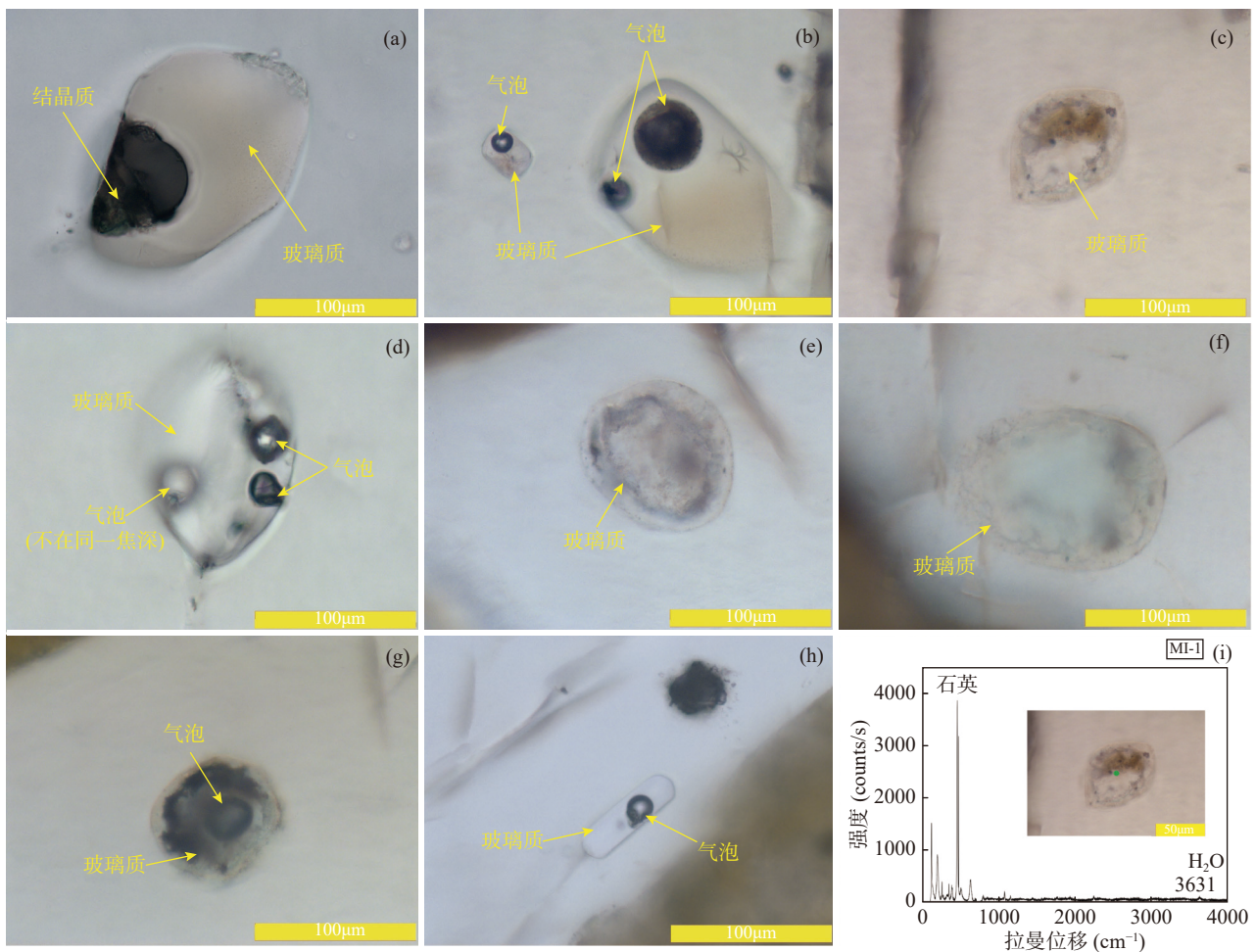
3.2.1 熔体包裹体岩相学特征

对采集样品的包裹体薄片进行镜下显微观察,熔体包裹体较发育,呈孤立状随机分布在石英斑晶的晶格缺陷中,未见到边界层、破裂或泄露等明显的

成分改造现象,表现出原生成因的岩相学特征^[7,42]。熔体包裹体颜色复杂,呈无色或淡黄色,其形态具有多样性,发育多边形(图5中a,b)、橄榄球形(图5中c,d)及椭圆形(图5e),直径为30~165μm。根据熔体包裹体相态特征,可将其划分为三类:①玻璃质+结晶质熔体包裹体(图5a);②玻璃质+气泡熔体包裹体(图5中b,d);③玻璃质熔体包裹体(图5中c,e)。熔体包裹体内部不含或只含少量真空气泡,属于冷却速率较快的喷发火山岩相^[6,43-44]。其中,呈孤立状分布在石英晶屑中、无破裂和泄露现象、不含或仅含单个气泡的熔体包裹体是岩浆迅速淬火冷凝而成,所捕获的熔体没有发生物理或化学成分改造,能代表矿物结晶时周围的熔体特征。

3.2.2 熔体包裹体拉曼光谱特征

髫髻山组凝灰岩中9个熔体包裹体样品的显微激光拉曼光谱测试结果显示:各熔体包裹体在3100~



a 为玻璃质+结晶质熔体包裹体; b、d、g、h 为玻璃质+气泡熔体包裹体; c、e、f 为玻璃质熔体包裹体; i 为熔体包裹体 MI-1 减基线后的拉曼光谱图。

图5 熔体包裹体镜下照片及熔体包裹体显微激光拉曼光谱图

Fig. 5 Microscopic photos showing characteristics of the melt inclusions and Raman spectrum of the melt inclusions.

3800 cm^{-1} 处均检测到水峰, 未检测到 CO_2 等其他挥发组分 (图 5f)。根据鲍文反应序列^[45], 石英形成于岩浆分离结晶作用晚期, 其捕获的熔体包裹体组成接近于喷发前的熔浆成分, 熔体包裹体中挥发份含量可以代表喷发前岩浆中挥发份含量^[2]。

3.2.3 凝灰岩熔体包裹体水含量特征

按照 2.3.2 节所述步骤对 9 个熔体包裹体样品的显微激光拉曼图谱进行处理, 并将处理结果 (即 A_{WF} 、 A_{LF}) 代入建立的水含量标定曲线方程, 即 2.4.3 中的方程 (2), 使用 Excel 进行计算, 得到的熔体包裹体水含量结果列于表 4。测定结果显示, 柳江盆地髻髻山组凝灰岩石英晶屑中熔体包裹体水含量为 0.99% ~ 4.98%, 平均含量为 2.62% (表 4)。

根据李福春等^[1]的熔体包裹体水含量统计数据, 大多数超基性基性岩浆中的水含量在 0 ~ 0.8%; 大部分中性岩浆水含量为 0.4% ~ 2.8%, 平均为 2.26%; 酸性岩浆水含量范围主要集中在 0.8% ~ 5.6%, 平均为 2.712%。对比测定结果与统计数据可以看出, 柳江盆地髻髻山组下部凝灰岩中熔体包裹体呈现高水含量的特点, 反映了岩浆演化后期为酸性岩浆, 这与岩石地球化学特征反映的岩浆性质一致, 进一步验证了该时期研究区存在由地壳浅部酸性岩浆活动引发的火山爆发。

柳江盆地位于燕山褶皱造山带东段 (图 1a), 在中侏罗世 (160±5Ma 前后) 受到燕山造山运动的影响强烈, 研究区处于大陆边缘活动阶段 (图 4d), 上地幔发生部分熔融^[25, 40-41], 形成的岛弧拉斑玄武质岩浆随着基性矿物的分离结晶, 逐渐向富硅、富水的酸性岩浆演化。水含量的增加促进了斜长石等矿物的分离结晶, 导致负 Eu 异常 (图 4c) 的形成^[46]; 高含水量的岩浆也可以促进流体相的形成, 使得大离子亲石元素更容易在岩浆中富集, 而高场强元素则难以进入流体相而在残余熔体中表现为亏损^[47]

(图 4b), 从而使其形成的火山岩具有特定的地球化学特征。此外, 水作为岩浆中最主要的挥发份, 控制着岩浆的脱气过程, 从而显著影响了岩浆系统的喷发动力^[43, 48]。根据样品的熔体包裹体水含量测定结果, 可以推测, 高水含量岩浆是研究区髻髻山期早期爆发性火山喷发的重要驱动因素之一。

4 结论

柳江盆地髻髻山组下部发育流纹质岩屑-晶屑凝灰岩, 在地球化学上表现出富水酸性岩浆的特征: 大离子亲石元素 (LILEs) 富集, 高场强元素 (HFSEs) 亏损, 稀土元素 (REEs) 配分模式呈现轻稀土 (LREEs) 富集、重稀土 (HREEs) 亏损的特点, 并出现负 Eu 异常和明显 Pb 正异常、Sr 负异常, 代表了研究区髻髻山期早期的岩浆特征。基于人工合成标样, 本文建立了显微激光拉曼光谱定量熔体包裹体水含量标定曲线, 并对柳江盆地髻髻山组下部凝灰岩石英晶屑内的熔体包裹体开展了水含量定量分析。测定结果表明, 该凝灰岩中熔体包裹体水含量为 0.99% ~ 4.98%, 平均为 2.62%, 介于酸性岩浆水含量范围, 指示了研究区髻髻山期早期为富水酸性岩浆。凝灰岩地球化学特征和熔体包裹体水含量测定结果均反映了柳江盆地髻髻山早期岩浆具有富水、富硅的特点。结合样品的熔体包裹体水含量测定结果和大规模火山喷发背景, 推测高水含量岩浆可能是导致此次爆发性火山喷发的重要条件之一。

今后的研究中, 可利用显微激光拉曼光谱法对研究区髻髻山期不同阶段的火山岩开展水含量系统分析, 这对于探讨燕山造山带髻髻山期火山岩成因和岩浆演化具有重要意义。

致谢: 感谢中国科学技术大学壳幔物质与环境重点实验室 (合肥) 高晓英教授团队提供的帮助。

表 4 髻髻山组凝灰岩中熔体包裹体 LF、WF 积分面积及水含量计算结果

Table 4 Integrated areas of LF and WF, and water content of the melt inclusions in tuff of the Tiaojishan Formation.

包裹体样品编号	熔体包裹体类型	A_{LF}	A_{WF}	$A_{\text{WF}}/A_{\text{LF}}$	峰位 (cm^{-1})	$C_{\text{H}_2\text{O}}$ (%)
MI-1	玻璃质	120.2732	203.0257	1.6880	3631	2.13
MI-2	玻璃质	119.9589	208.9559	1.7419	3631	2.19
MI-3	玻璃质	297.2329	233.0028	0.7839	3643	0.99
MI-4	玻璃质	198.5294	276.1755	1.3911	3636	1.75
MI-5	玻璃质	180.3690	306.9109	1.7016	3631	2.14
MI-6	玻璃质+气泡	78.6287	288.6345	3.6709	3636	4.63
MI-7	玻璃质+气泡	222.9093	237.9510	1.0675	3637	1.35
MI-8	玻璃质+气泡	526.2989	1446.2396	2.7479	3541	3.46
MI-9	玻璃质+结晶质	186.4130	737.1156	3.9542	3568	4.98

Geochemical Characteristics and Water Content of Melt Inclusions in the Tuff of the Tiaojishan Formation, Liujiang Basin

ZHAO Huizhen^{1,2}, CHEN Yong^{1,2*}, TU Cong³, FENG Yanwei^{1,2}

(1. National Key Laboratory of Deep Oil and Gas, China University of Petroleum (East China), Qingdao 266580, China;

2. School of Geosciences, China University of Petroleum (East China), Qingdao 266580, China;

3. School of Earth and Space Sciences, University of Science and Technology of China, Hefei 230026, China)

HIGHLIGHTS

- (1) The establishment of a calibration curve is crucial for the quantitative determination of water content in melt inclusions using laser Raman spectroscopy.
- (2) The water content of melt inclusions has a strong linear relationship with Raman spectroscopy parameters, allowing a calibration curve to be established with only a few standard samples.
- (3) The average water content of melt inclusions in the tuffaceous rocks from the Tiaojishan Formation in the Liujiang Basin is 2.62%, indicating an acidic, water-enriched magmatic system.

ABSTRACT: Water, as the primary volatile component in magmatic systems, has a significant impact on the formation and evolution of magma. The Tiaojishan Formation igneous rocks in the Liujiang Basin are significant products of Yanshanian volcanic activity. Although previous studies have extensively explored their geochemical characteristics, the water content of the magma in the Liujiang Basin during Yanshanian volcanic activity remains unclear. Melt inclusions, which capture the original magmatic information, serve as the most direct samples for determining the water content of magma. Based on geochemical analysis, this study quantitatively determines the water content in melt inclusions using laser Raman spectroscopy with standard samples. The results show that the lower tuff samples of the Tiaojishan Formation are characterized by high Si and Al contents, enrichment in LILEs, depletion in HFSEs, enrichment in LREEs, and depletion in HREEs. The water content in melt inclusions reveals a range of 0.99% to 4.98%, with an average of 2.62%. These characteristics jointly indicate the water-enriched acidic magmatic activity during the early Tiaojishan period in this area. Combining the water content of melt inclusions with the large-scale volcanic eruptions in the stage, this study suggests that high water content in the magma enhanced the eruptive dynamics of the magmatic system, making it a contributing factor to the large-scale volcanic eruption. The BRIEF REPORT is available for this paper at <http://www.ykcs.ac.cn/en/article/doi/10.15898/j.ykcs.202404030074>.

KEY WORDS: Liujiang Basin; Tiaojishan Formation; tuff; melt inclusions; water content; laser Raman spectroscopy

BRIEF REPORT

Significance: Water (H_2O) is the most significant volatile component in natural magmatic systems, playing a vital role in shaping the physical and chemical properties of magma. Its presence significantly affects magma viscosity, melting point, and crystallization. Therefore, water exerts a controlling influence over the overall trends of magmatic differentiation and evolution, guiding the chemical evolution of the magma as it cools and solidifies over time^[1-3]. Melt inclusions, as snapshots of magma during geological periods, can preserve the original characteristics of the magma, making them the most direct geological samples for assessing water content in magmas^[6-8]. Studying the water content in melt inclusions not only reveals the processes of magmatic differentiation and evolution, but also provides critical evidence for understanding the characteristics of magmatic activity.

Despite the importance of water in influencing magmatic processes, current studies on the water content in Mesozoic volcanic rocks, specifically within the Yanshanian Orogen, remain limited. The Tiaojishan Formation volcanics are among the most representative calc-alkaline volcanic rocks of the Mesozoic Yanshanian Orogen, marking the onset of large-scale volcanic eruptions during the Yanshan period^[20]. Although extensive research has focused on the geochemistry of these volcanic rocks, the water content within the Tiaojishan Formation's volcanics is not well-understood^[21-25]. This knowledge gap limits our understanding of how water influences magma behavior during large-scale volcanic events of the Yanshan period.

This study addresses the gap by quantifying the water content in melt inclusions from tuff in the Lower Tiaojishan Formation (J_2t), an early volcanic product of the Yanshanian Orogen. Utilizing micro-laser Raman spectroscopy, which allows high-resolution, rapid, and non-destructive water content measurement, the study provides quantitative petrochemical data essential for understanding magmatic processes in this region. Our findings advance the understanding of water's role in regional magmatic differentiation, contributing key insights into the volcanic activity of the Yanshanian Orogen.

Methods: The tuff samples used in this study were collected from the lower part of the Tiaojishan Formation outcrop in the Liujiang Basin, Qinhuangdao, Hebei Province. All experiments were conducted at the National Key Laboratory of Deep Oil and Gas of China University of Petroleum (East China). A Leica DM2700P microscope was used for microscopic observation, while IRIS Intrepid II XSP ICP-OES and ELAN9000 ICP-MS were employed for the analysis of major and trace elements. For microscopic laser Raman spectroscopy testing, a LABRAM HR EVO Laser Raman Spectrometer manufactured by HORIBA FRANCE SAS was utilized.

The microscopic laser Raman spectroscopy experiments are conducted with a laser power of 30mW, an integration time of 30s, and each measurement was integrated three times. To enhance the accuracy of the experimental outcomes, the Raman spectra are subjected to a detailed processing procedure. This process involves several critical steps, beginning with intensity correction, which adjusts the spectral data to account for any fluctuations in laser power or detector sensitivity. Following this, baseline correction is applied to remove any background noise or interference, ensuring that the true signal is accurately isolated. Finally, bands integration is performed, where the area under specific peaks within the spectrum is calculated, allowing for a precise quantification of the target components. Acidic silicate glass exhibits a strong LF_{470} Raman peak height/intensity (Fig.2), and A_{WF}/A_{LF} is preferentially selected as the optimal calibration parameter^[11,19]. Subsequently, a crucial calibration curve for water content is established with the glass standards synthesized by Professor Gao Xiaoying's team from University of Science and Technology of China. Nine well-preserved primary melt inclusions were carefully selected under a microscope for analysis. These inclusions underwent rigorous testing and detailed data processing, during which their water content was meticulously calculated based on the data.

Data and Results: The experimental results obtained by petrographic observation, analysis of major and trace elements and microscopic laser Raman spectroscopy are shown in the following two parts.

(1) Petrological and geochemical characteristics

The tuff from the lower part of the Tiaojishan Formation is classified as Rhyolite lithic-crystalline tuff, characterized by a blocky texture. It predominantly comprises crystal fragments (35%), rock fragments (25%) and matrix (40%). The crystal fragments are mainly composed of quartz and feldspar, with particle sizes reaching up to 1.8mm; The rock fragments consist mainly of rhyolite debris, with particle sizes ranging from 0.5 to 2mm. The matrix is composed of fine dust and volcanic ash.

The major and trace element analysis results of the whole-rock tuff samples are presented in Table 2 and Table 3, respectively. The samples are marked by high concentrations of Si and Al, enrichment in large ion lithophile elements (LILEs), and depletion in high field strength elements (HFSEs) (Fig.4b). The samples also exhibit enrichment in light rare earth elements (LREEs) and depletion in heavy rare earth elements (HREEs) (Fig.4c), along with a negative Eu anomaly and low Sr content. The TAS diagram (Fig.4a) positions the tuff within the rhyolite field, suggesting its formation is closely associated with acidic magmatic activity. The Ta/Yb-Th/Yb diagram (Fig.4d) places the samples within the active continental margin, inferring that the study area was significantly influenced by oceanic subduction and magmatic activity during this period.

(2) Characteristics of melt inclusions and water content in the tuff

The melt inclusions are primarily isolated and randomly distributed within the lattice defects of quartz phenocrysts, indicative of their primary magmatic origin. These inclusions appear colorless or pale yellow, and exhibit a variety of morphologies, including polygonal (Fig.5a, b), ellipsoidal (Fig.5c, d), and oval shapes (Fig.5e), with diameters varying between 30 μ m and 165 μ m. Based on their phase characteristics, the melt inclusions can be categorized into three types: (1)glassy+crystalline melt inclusions (Fig.5a), (2)glassy+bubble-bearing melt inclusions (Fig.5b, d), and (3)glassy melt inclusions (Fig.5c, e). The melt inclusions contain either no or only a few small vapor bubbles, indicating their formation in a volcanic facie with a relatively rapid cooling rate^[6,43-44].

Water peaks were identified at 3100–3800 cm^{-1} ; in the nine melt inclusions, with no detection of CO_2 or other volatiles (Fig.5f). According to Bowen's reaction series^[45], quartz forms in the late stage of magmatic fractional crystallization, and the composition of melt inclusions captured by quartz closely resembles the pre-eruption magma. In other words, the water content in these melt inclusions reflects the water content in the magma before the eruption^[2].

The calibration equation for water content is $C_{\text{H}_2\text{O}}=1.26\times(A_{\text{WF}}/A_{\text{LF}})$ with $R^2=0.998$ (Fig.3). After processing the micro-laser Raman spectra of the nine melt inclusions, the results (A_{WF} , A_{LF}) are substituted into the water content calibration curve equation [Equation (2)]. Calculations were performed using Excel, and the water content results for the melt inclusions are presented in Table 4. The results indicate that the water content in the melt inclusions within quartz crystal fragments in the tuff from the Tiaojishan Formation in the Liujiang Basin ranges from 0.99% to 4.98%, with an average of 2.62% (Table 4). A comparison with statistical data provided by Li et al.^[1] shows that most ultrabasic to basic magmas have a water content ranging from 0 to 0.8%, while intermediate magmas typically range from 0.4% to 2.8%, with an average of 2.26%, and the water content in acidic magmas generally falls between 0.8% and 5.6%, with an average of 2.712%. The high-water content observed in the melt inclusions from the lower Tiaojishan Formation tuff in the Liujiang Basin suggests that the magma transited into an acidic state in the late stage of its evolution.

参考文献

- [1] 李福春, 朱金初, 金章东. 岩浆中主要挥发份含量——熔融包裹体和淬火玻璃证据[J]. 地质地球化学, 2000, 28(2): 8-13.
Li F C, Zhu J C, Jin Z D. Contents of main volatiles in magma: Evidence from melt inclusions and quenched glasses[J]. *Geology Geochemistry*, 2000, 28(2): 8-13.
- [2] 李霓, 孙嘉祥. 火山岩中熔体包裹体研究进展[J]. 矿物岩石地球化学通报, 2018, 37(3): 414-423.
Li N, Sun J X. A review on research progress of melt inclusion in volcanic rocks[J]. *Bulletin of Mineralogy, Petrology and Geochemistry*, 2018, 37(3): 414-423.
- [3] Forte P, Castro J M. H₂O-content and temperature limit the explosive potential of rhyolite magma during Plinian eruptions[J]. *Earth and Planetary Science Letters*, 2019, 506: 157-167.
- [4] Roedder E. Origin and significance of magmatic inclusions[J]. *Bulletin de Mineralogie*, 1979, 102(5): 487-510.
- [5] Roedder E. Fluid inclusions[M]//Ribbe P H, ed. *Reviews in mineralogy* (Vol. 12). Washington DC: Mineralogical Society of America, 1984.
- [6] 王蝶, 卢焕章, 单强. 岩浆熔体包裹体研究进展[J]. 岩石学报, 2017, 33(2): 653-666.
Wang D, Lu H Z, Shan Q. Advances on melt inclusion studies[J]. *Acta Petrologica Sinica*, 2017, 33(2): 653-666.
- [7] Bennett E N, Jenner F E, Millet M A, et al. Deep roots for mid-ocean-ridge volcanoes revealed by plagioclase-hosted melt inclusions[J]. *Nature*, 2019, 572(7768): 235-239.
- [8] Metrich N, Wallace P J. Volatile abundances in basaltic magmas and their degassing paths tracked by melt inclusions[J]. *Reviews in Mineralogy and Geochemistry*, 2008, 69(1): 363-402.
- [9] Esposito R, Hunter J, Schiffbauer J D, et al. An assessment of the reliability of melt inclusions as recorders of the pre-eruptive volatile content of magmas[J]. *American Mineralogist*, 2014, 99(5-6): 976-998.
- [10] 丁一, 刘吉强, 宗统, 等. 熔体包裹体挥发份应用的研究进展[J]. 岩石矿物学杂志, 2019, 38(6): 897-913.
Ding Y, Liu J Q, Zong T, et al. A review on the application of volatiles in melt inclusions[J]. *Acta Petrologica Sinica*, 2019, 38(6): 897-913.
- [11] 高晓英, 涂聪, 孟子岳. 激光拉曼光谱仪定量测定硅酸盐熔体包裹体中水含量及其地质应用[J]. 地球科学, 2022, 47(10): 3616-3632.
Gao X Y, Tu C, Meng Z Y. Geological application of Raman spectroscopy to quantify trace water concentrations in silicate glasses[J]. *Earth Science*, 2022, 47(10): 3616-3632.
- [12] 王玉琪, 丁兴, 邸健, 等. 激光拉曼快速标定花岗质玻璃的水含量[J]. 地球化学, 2023, 52(2): 250-260.
Wang Y Q, Ding X, Di J, et al. Rapid analysis of water content in granitic glass using *in situ* Raman spectroscopy[J]. *Geochimica*, 2023, 52(2): 250-260.
- [13] 孟庆国, 刘昌岭, 李承峰, 等. X射线粉晶衍射-拉曼光谱法研究含甲烷双组分水合物结构及谱学特征[J]. 岩矿测试, 2021, 40(1): 85-94.
Meng Q G, Liu C L, Li C F, et al. Study on the structure and spectroscopic characteristics of methane-containing binary hydrates using X-ray powder diffraction-Raman spectroscopy[J]. *Rock and Mineral Analysis*, 2021, 40(1): 85-94.
- [14] 杨春梅, 黄梓芸, 覃静雯, 等. 应用钻石观测仪-红外光谱仪-激光诱导击穿光谱仪鉴定无机材料充填翡翠[J]. 岩矿测试, 2022, 41(2): 281-290.
Yang C M, Huang Z Y, Qin J W, et al. Identification of inorganic material-filled jadeite using diamond observation instrument-infrared spectrometer-laser-induced breakdown spectrometer[J]. *Rock and Mineral Analysis*, 2022, 41(2): 281-290.
- [15] 范晨子, 孙冬阳, 赵令浩, 等. 激光剥蚀电感耦合等离子体质谱法微区原位定量分析锂铍矿物化学成分[J]. 岩矿测试, 2024, 43(1): 87-100.
Fan C Z, Sun D Y, Zhao L H, et al. Micro-area *in-situ* quantitative analysis of chemical composition of lithium-beryllium minerals using laser ablation inductively coupled plasma mass spectrometry[J]. *Rock and Mineral Analysis*, 2024, 43(1): 87-100.
- [16] Thomas R. Determination of water contents of granite melt inclusions by confocal laser Raman microprobe spectroscopy[J]. *American Mineralogist*, 2000, 85(5-6): 868-872.
- [17] Chabiron A, Pironon J, Massare D. Characterization of water in synthetic rhyolitic glasses and natural melt

- inclusions by Raman spectroscopy[J]. *Contributions to Mineralogy and Petrology*, 2004, 146: 485–492.
- [18] 陈勇. 流体包裹体激光拉曼光谱分析方法及应用[M]. 北京: 中国石油大学出版社, 2015.
- Chen Y. Raman spectroscopy for fluid inclusion analysis and applications[M]. Beijing: China University of Petroleum Press, 2015.
- [19] Tu C, Meng Z Y, Gao X Y, et al. Quantification of water content and speciation in synthetic rhyolitic glasses: Optimising the analytical method of confocal Raman spectrometry[J]. *Geostandards and Geoanalytical Research*, 2023, 47(3): 549–567.
- [20] 赵越, 徐刚, 张拴宏, 等. 燕山运动与东亚构造体制的转变[J]. *地质前缘*, 2004, 11(3): 319–328.
- Zhao Y, Xu G, Zhang S H, et al. Yanshan movement and conversion of tectonic regimes in East Asia[J]. *Earth Science Frontiers*, 2004, 11(3): 319–328.
- [21] 李伍平, 赵越, 李献华, 等. 燕山造山带中一晚侏罗世髻髻山期(蓝旗期)火山岩的成因及其动力学意义[J]. *岩石学报*, 2007, 23(3): 557–564.
- Li W P, Zhao Y, Li X H, et al. Genesis and dynamic significance of the middle-late Jurassic Tiaojishan (Lanqi) volcanic rocks in the Yanshan orogenic belt[J]. *Acta Petrologica Sinica*, 2007, 23(3): 557–564.
- [22] 段超, 毛景文, 谢桂青, 等. 太行山北段木吉村髻髻山组安山岩锆石 U-Pb 年龄和 Hf 同位素特征及其对区域成岩成矿规律的指示[J]. *地质学报*, 2016, 90(2): 250–266.
- Duan C, Mao J W, Xie G Q, et al. Zircon U-Pb age and Hf isotopic characteristics of the Tiaojishan Formation andesite in Mujicun, Northern Taihang Mountains, and its implications for regional magmatism and metallogeny[J]. *Acta Geologica Sinica*, 2016, 90(2): 250–266.
- [23] 于海飞, 张志诚, 帅歌伟, 等. 北京十三陵—西山髻髻山组火山岩年龄及其地质意义[J]. *地质论评*, 2016, 62(4): 807–826.
- Yu H F, Zhang Z C, Shuai G W, et al. Age and geological significance of the Tiaojishan Formation volcanic rocks in the Shisanling—Xishan area, Beijing[J]. *Geological Review*, 2016, 62(4): 807–826.
- [24] 李斌, 陈井胜, 刘森, 等. 辽西髻髻山组的形成时代及地球化学特征[J]. *地质论评*, 2019, 65(S1): 2.
- Li B, Chen J S, Liu M, et al. Formation age and geochemical characteristics of the Tiaojishan Formation in Western Liaoning[J]. *Geological Review*, 2019, 65(S1): 2.
- [25] 赵瑞鹏, 陈亮, 刘道宏, 等. 河北秦皇岛石门寨中生代火山岩的地球化学特征和锆石 LA-ICP-MS U-Pb 年龄[J]. *地质论评*, 2019, 65(4): 929–947.
- Zhao R P, Chen L, Liu D H, et al. Geochemical characteristics and zircon LA-ICP-MS U-Pb age of Mesozoic volcanic rocks in Shimen Village, Qinhuangdao, Hebei[J]. *Geological Review*, 2019, 65(4): 929–947.
- [26] 吴孔友, 冀国盛. 秦皇岛地区地质认识实习指导书[M]. 北京: 中国石油大学出版社, 2007.
- Wu K Y, Ji G S. Field guide for geological understanding practice in the Qinhuangdao area[M]. Beijing: China University of Petroleum Press, 2007.
- [27] 郑亚东, Davis G A, 王琮, 等. 燕山带中生代主要构造事件与板块构造背景问题[J]. *地质学报*, 2000, 74(4): 289–302.
- Zheng Y D, Davis G A, Wang C, et al. Major Mesozoic tectonic events and plate tectonic background of the Yanshan belt[J]. *Acta Geologica Sinica*, 2000, 74(4): 289–302.
- [28] Mysen B O, Virgo D, Scarfe C M. Relations between the anionic structure and viscosity of silicate melts—A Raman spectroscopic study[J]. *American Mineralogist*, 1980, 65(7–8): 690–710.
- [29] Sharma S K, Mammone J F, Nicol M F. Raman investigation of ring configurations in vitreous silica[J]. *Nature*, 1981, 292(5819): 140–141.
- [30] McMillan P. Structural studies of silicate glasses and melts—Applications and limitations of Raman spectroscopy[J]. *American Mineralogist*, 1984, 69(7–8): 622–644.
- [31] Matson D W, Sharma S K, Philpotts J A. Raman spectra of some tectosilicates and of glasses along the orthoclase-anorthite and nepheline-anorthite joins[J]. *American Mineralogist*, 1986, 71(5–6): 694–704.
- [32] Mysen B O, Virgo D, Seifert F A. The structure of silicate melts: Implications for chemical and physical properties of natural magma[J]. *Reviews of Geophysics*, 1982, 20(3): 353–383.

- [33] McMillan P F, Remmele R L. Hydroxyl sites in SiO₂ glass: A note on infrared and Raman spectra[J]. *American Mineralogist*, 1986, 71(5-6): 772-778.
- [34] Mysen B O, Holtz F, Pichavant M, et al. Solution mechanisms of phosphorus in quenched hydrous and anhydrous granitic glass as a function of peraluminosity [J]. *Geochimica et Cosmochimica Acta*, 1997, 61(18): 3913-3926.
- [35] Long D A. Raman spectroscopy[M]. New York: McGraw-Hill, 1977.
- [36] Irving A J, Frey F A. Trace element abundances in megacrysts and their host basalts: Constraints on partition coefficients and megacryst genesis[J]. *Geochimica et Cosmochimica Acta*, 1984, 48(6): 1201-1221.
- [37] Sun S S, McDonough W F. Chemical and isotopic systematics of oceanic basalts: Implications for mantle composition and processes[J]. *Geological Society Special Publications*, 1989, 42(1): 313-345.
- [38] Pearce J A. Trace element characteristics of lavas from destructive plate boundaries[M]//Thorpe R S. Orogenic andesites and related rocks. John Wiley & Sons, 1982: 528-548.
- [39] McDonough W F, Sun S S. The composition of the Earth[J]. *Chemical Geology*, 1995, 120(3-4): 223-253.
- [40] 朱日祥, 徐义刚. 西太平洋板块俯冲与华北克拉通破坏[J]. *中国科学: 地球科学*, 2019, 49(9): 1346-1356.
Zhu R X, Xu Y G. The subduction of the west Pacific plate and the destruction of the North China Craton[J]. *Science China Earth Sciences*, 2019, 49(9): 1346-1356.
- [41] 牛俊杰. 下地壳埃达克质岩浆房的发现: 来自角闪石循环晶的证据[D].北京: 中国地质大学(北京), 2020.
Niu J J. The hidden Adakitic magma reservoir in the lower crust revealed by amphibole antecrysts[D]. Beijing: China University of Geosciences (Beijing), 2020.
- [42] 卢焕章, 范宏瑞, 倪培, 等. 流体包裹体[M]. 北京: 科学出版社, 2004.
Lu H Z, Fan H R, Ni P, et al. Fluid inclusions[M]. Beijing: Science Press, 2004.
- [43] 李霓, 樊祺诚, 孙谦, 等. 熔体包裹体对长白山天池火山千年大喷发的指示意义[J]. *岩石学报*, 2008, 24(11): 2604-2614.
Li N, Fan Q C, Sun Q, et al. The implication of melt inclusion for the millennium eruption of Changbaishan Tianchi volcano[J]. *Acta Petrologica Sinica*, 2008, 24(11): 2604-2614.
- [44] 张道涵, 魏俊浩, 付乐兵, 等. 熔体包裹体的形成、改造和分析方法及其矿床学应用[J]. *地球科学*, 2017, 42(6): 990-1007.
Zhang D H, Wei J H, Fu L B, et al. Formation, modification and analytical techniques of melt inclusion, and their applications in economic geology[J]. *Earth Science*, 2017, 42(6): 990-1007.
- [45] Bowen N L. The evolution of the igneous rocks[M]. Princeton: Princeton University Press, 1928.
- [46] Hartung E, Weber G, Caricchi L. The role of H₂O on the extraction of melt from crystallising magmas[J]. *Earth and Planetary Science Letters*, 2019, 508: 85-96.
- [47] Cerpa N G, Wada I, Wilson C R. Effects of fluid influx, fluid viscosity, and fluid density on fluid migration in the mantle wedge and their implications for hydrous melting[J]. *Geosphere*, 2019, 15(1): 1-23.
- [48] Rasmussen D J, Plank T A, Roman D C, et al. Magmatic water content controls the pre-eruptive depth of arc magmas[J]. *Science*, 2022, 375(6585): 1169-1172.